Transition of yeast Can1 transporter to the inward-facing state unveils an α-arrestin target sequence promoting its ubiquitylation and endocytosis

Christos Gournas[a], Elie Saliba[a], Eva-Maria Krammer[b], Céline Barthelemy[a], Martine Prévost[b], and Bruno André[a,*]

[a]Molecular Physiology of the Cell, Université Libre de Bruxelles, 6041 Gosselies, Belgium; [b]Structure and Function of Biological Membranes, Université Libre de Bruxelles, 1050 Brussels, Belgium

ABSTRACT **Substrate-transport–elicited endocytosis is a common control mechanism of membrane transporters avoiding excess uptake of external compounds, though poorly understood at the molecular level. In yeast, endocytosis of transporters is triggered by their ubiquitylation mediated by the Rsp5 ubiquitin-ligase, recruited by α-arrestin–family adaptors. We here report that transport-elicited ubiquitylation of the arginine transporter Can1 is promoted by transition to an inward-facing state. This conformational change unveils a region of the N-terminal cytosolic tail targeted by the Art1 α-arrestin, which is activated via the TORC1 kinase complex upon arginine uptake. Can1 mutants altered in the arginine-binding site or a cytosolic tripeptide sequence permanently expose the α-arrestin–targeted region so that Art1 activation via TORC1 is sufficient to trigger their endocytosis. We also provide evidence that substrate-transport elicited endocytosis of other amino acid permeases similarly involves unmasking of a cytosolic Art1-target region coupled to activation of Art1 via TORC1. Our results unravel a mechanism likely involved in regulation of many other transporters by their own substrates. They also support the emerging view that transporter ubiquitylation relies on combinatorial interaction rules such that α-arrestins, stimulated via signaling cascades or in their basal state, recognize transporter regions permanently facing the cytosol or unveiled during transport.**

Monitoring Editor
Sandra Lemmon
University of Miami

Received: Feb 16, 2017
Revised: Aug 10, 2017
Accepted: Aug 11, 2017

INTRODUCTION

The plasma membrane of all cells contains a wide variety of transporters, many of which are subject to tight regulation. A common mechanism for inhibiting the function of these proteins is selective sorting into endocytic vesicles, followed by delivery to the lysosome for degradation. This down-regulation has been particularly well studied in the yeast *Saccharomyces cerevisiae* (Léon and Haguenauer-Tsapis, 2009; Lauwers *et al.*, 2010; MacGurn *et al.*, 2012). Endocytosis of most yeast transporters is triggered by their ubiquitylation via the HECT-type ubiquitin (Ub) ligase Rsp5. Recognition of target transporters by Rsp5 requires adaptors of the α-arrestin family (Lin *et al.*, 2008; Nikko *et al.*, 2008; Becuwe *et al.*, 2012; Merhi and André, 2012; Alvaro *et al.*, 2014). These proteins are distantly related to the ß-arrestins controlling G-protein-coupled receptors and likely emerged before them during evolution (Alvarez, 2008). Yeast possesses 14 α-arrestin–family proteins (Art1 to -10, Bul1 to -3, Spo23), all of which contain PPxY motifs recognized by the WW domains of Rsp5. The α-arrestins of animal cells, named ARRDCs (arrestin domain–containing proteins), also contain PPxY motifs, and several can interact with Rsp5-related Ub ligases of the Nedd4 family (Patwari and Lee, 2012). The α-arrestin TXNIP is reported to bind to the Glut1 glucose transporter and to stimulate its endocytosis (Wu *et al.*, 2013).

This article was published online ahead of print in MBoC in Press (http://www.molbiolcell.org/cgi/doi/10.1091/mbc.E17-02-0104) on August 16, 2017.

*Address correspondence to: Bruno André (Bruno.Andre@ulb.ac.be).

Abbreviations used: APC, amino-acid-polyamine-organocation; ARRDCs, arrestin domain–containing proteins; TM, ransmembrane segment; TORC1, target of rapamycin complex 1; Ub, ubiquitin.

Recent studies in yeast have shown that stimulation of transporter ubiquitylation can result from direct control of α-arrestins according to the metabolic status of the cell. For instance, the Jen1 lactate transporter is highly expressed in cells growing on lactate as a carbon source. In these cells, the Rod1/Art4 α-arrestin required for Jen1 ubiquitylation is phosphorylated by the Snf1 kinase, and this promotes its inhibitory association with the 14-3-3 proteins. Upon glucose addition, Rod1 is rapidly dephosphorylated, dissociates from the 14-3-3s, and can thus promote Jen1 ubiquitylation via Rsp5 (Becuwe *et al.*, 2012). A similar mechanism accounts for down-regulation of the general amino acid permease Gap1. This transporter is highly expressed in cells grown on a poor nitrogen source. Under these conditions, the redundant Bul1 and Bul2 α-arrestins required for Gap1 ubiquitylation are phosphorylated by the Npr1 kinase, and this promotes their inhibitory binding to the 14-3-3s. Upon addition of ammonium, a preferred nitrogen source, the TORC1 kinase complex is stimulated and inhibits Npr1 by phosphorylation (Schmidt *et al.*, 1998). Furthermore, the Sit4 phosphatase dephosphorylates the Bul α-arrestins, which dissociate from the 14-3-3s and promote Gap1 ubiquitylation (Merhi and André, 2012). A short sequence present in the cytosolic N-terminal tail (N-tail) of Gap1 is essential to this ubiquitylation and is likely a permanently exposed binding site for the activated Buls (Ghaddar *et al.*, 2014b). Another amino acid permease controlled by the TORC1-Npr1 cascade is Can1, the arginine-specific permease, whose endocytosis requires the Art1 α-arrestin (Lin *et al.*, 2008; MacGurn *et al.*, 2011).

Another condition promoting ubiquitylation and endocytosis of several fungal transporters is transport of their own substrates. Inactive mutant transporters resist this transport-elicited down-regulation, and for some of them, it has been shown that this is not simply due to reduced substrate accumulation (Gournas *et al.*, 2016). Current models propose, rather, that substrate-transport–elicited endocytosis requires transition of the protein to a particular conformation prone to ubiquitylation (Gournas *et al.*, 2010; Keener and Babst, 2013; Ghaddar *et al.*, 2014b). The Gap1 and Can1 permeases have recently been reported to undergo transport-elicited endocytosis, via Bul1/2 and Art1, respectively (Ghaddar *et al.*, 2014b). However, the molecular mechanisms of transport-elicited ubiquitylation, likely shared by many other transporters of yeast and more complex species, remain elusive.

In this study we molecularly dissected the mechanisms inducing ubiquitylation and endocytosis of the Can1 permease during transport of its substrate arginine (Arg). We present evidence that efficient Can1 down-regulation requires transition of the transporter to an inward-facing conformation, causing exposure to the cytosol of a short N-tail sequence necessary for Art1-dependent ubiquitylation. In addition to this conformational signal, efficient Can1 down-regulation requires stimulation of Art1 via the TORC1-Npr1 cascade. Our results suggest that the ubiquitylation of transporters is regulated by modulation of their interaction with α-arrestins and that this relies on control of the α-arrestins themselves and/or on conformation-dependent exposure of their binding sites.

RESULTS

The Art1 and Bul α-arrestins promote Can1 ubiquitylation in response to arginine

Substrate-transport–elicited endocytosis of Can1, followed by its delivery to the vacuole, is readily observed after addition of Arg to cells grown on proline (Pro) as sole nitrogen source (Ghaddar *et al.*, 2014b; Figure 1, A and B). As expected, this down-regulation appeared largely defective in the hypomorphic *npi1(rsp5)* mutant where Rsp5 Ub ligase expression is reduced at least 20-fold (Springael and André, 1998) (Figure 1, A and B). As Can1 ubiquitylation has not been reported to date, we used immunoblotting to detect the ubiquitylated protein in cell extracts (Figure 1C). Arg addition induced the appearance of slowly migrating bands above the main Can1-GFP (green fluorescent protein) signal. These upper bands correspond to Can1-Ub conjugates, as they were barely detectable in the *npi1(rsp5)* mutant (Figure 1C) and not detected at all when all lysines (Lys) of the Can1 N-tail were replaced with arginines (see below). Furthermore, addition of Arg induced the appearance of Ub linked to pulled-down Can1-GFP, but not the Can1-GFP mutant with all N-tail Lys substituted (Figure 1D). We have previously reported that substrate-elicited down-regulation of Can1 depends on both permease activity and specificity (Ghaddar *et al.*, 2014b). After Arg addition, accordingly, the totally inactive Can1(T180R) deficient in substrate binding (Ghaddar *et al.*, 2014a) was not ubiquitylated and remained stable at the cell surface (Figure 1, E and F). Furthermore, the Can1(S176N,T456S) mutant previously shown to be converted into a Lys-specific permease (Ghaddar *et al.*, 2014a), was ubiquitylated and down-regulated in response to Lys instead of Arg (Figure 1, E and F).

As observed previously (Ghaddar *et al.*, 2014b), Arg-induced down-regulation of Can1 was impaired in a mutant lacking the Art1 α-arrestin (Figure 1, A, B, G, and H, and Supplemental Figure S1). In this strain, however, Can1 was still ubiquitylated in response to Arg, though much less efficiently (Figure 1C). Furthermore, quantification of fluorescence signals revealed significant internalization of Can1-GFP after Arg addition to *art1*Δ cells (Figure 1B), suggesting that additional α-arrestins can promote significant Can1 ubiquitylation and endocytosis. We next noticed that this Art1-independent Can1 ubiquitylation was more pronounced in cells grown on ammonium (Am) as sole nitrogen source (Figure 1G), a condition known to activate the redundant Bul1 and Bul2 α-arrestins via TORC1-dependent phosphoinhibition of the Npr1 kinase (Merhi and André, 2012). We thus hypothesized that the residual ubiquitylation and endocytosis of Can1 observed in the *art1*Δ mutant might depend on the Bul proteins. This was confirmed when we examined Can1 in the *art1*Δ *bul1*Δ *bul2*Δ triple mutant (Figure 1, G and H, and Supplemental Figure S1).

Can1 solely ubiquitylated via Art1 or Bul1/2 undergoes different fates after internalization

Although the Bul α-arrestins can promote efficient Can1 ubiquitylation in response to Arg, especially in cells grown on Am (Figure 1G), subsequent targeting to the vacuole was much less efficient than when ubiquitylation was mediated by Art1 alone (Figure 1H and Supplemental Figure, S1). We investigated this unexpected observation and found that upon Arg addition to *art1*Δ cells, Can1 was efficiently internalized but largely recycled to the cell surface via the Golgi. More specifically, in an *art1*Δ strain additionally lacking the Ypt6 Rab GTPase involved in endosome-to-Golgi recycling (Luo and Gallwitz, 2003) and known to promote cell-surface recycling of internalized permeases (Figure 2A; Nikko *et al.*, 2003; Lauwers *et al.*, 2009), Can1-GFP was targeted to the vacuole in a Bul1/2–dependent manner (Figure 2B and Supplemental Figure S2). The results thus indicate that in the *art1*Δ strain, Can1 is ubiquitylated via Bul1/2, internalized, and then recycles to the plasma membrane, probably by passing through the Golgi. In support of this view, we could observe a significant Bul1/2-dependent colocalization of Can1-GFP with the Sec7 Golgi marker 15 min after Arg addition to *art1*Δ cells (Figure 2C). In the *bul1*Δ *bul2*Δ strain, in contrast, internalized Can1 was efficiently targeted to the vacuole whether the cells were grown on Pro or Am, and this down-regulation depended on Art1 (Figure 1H). The

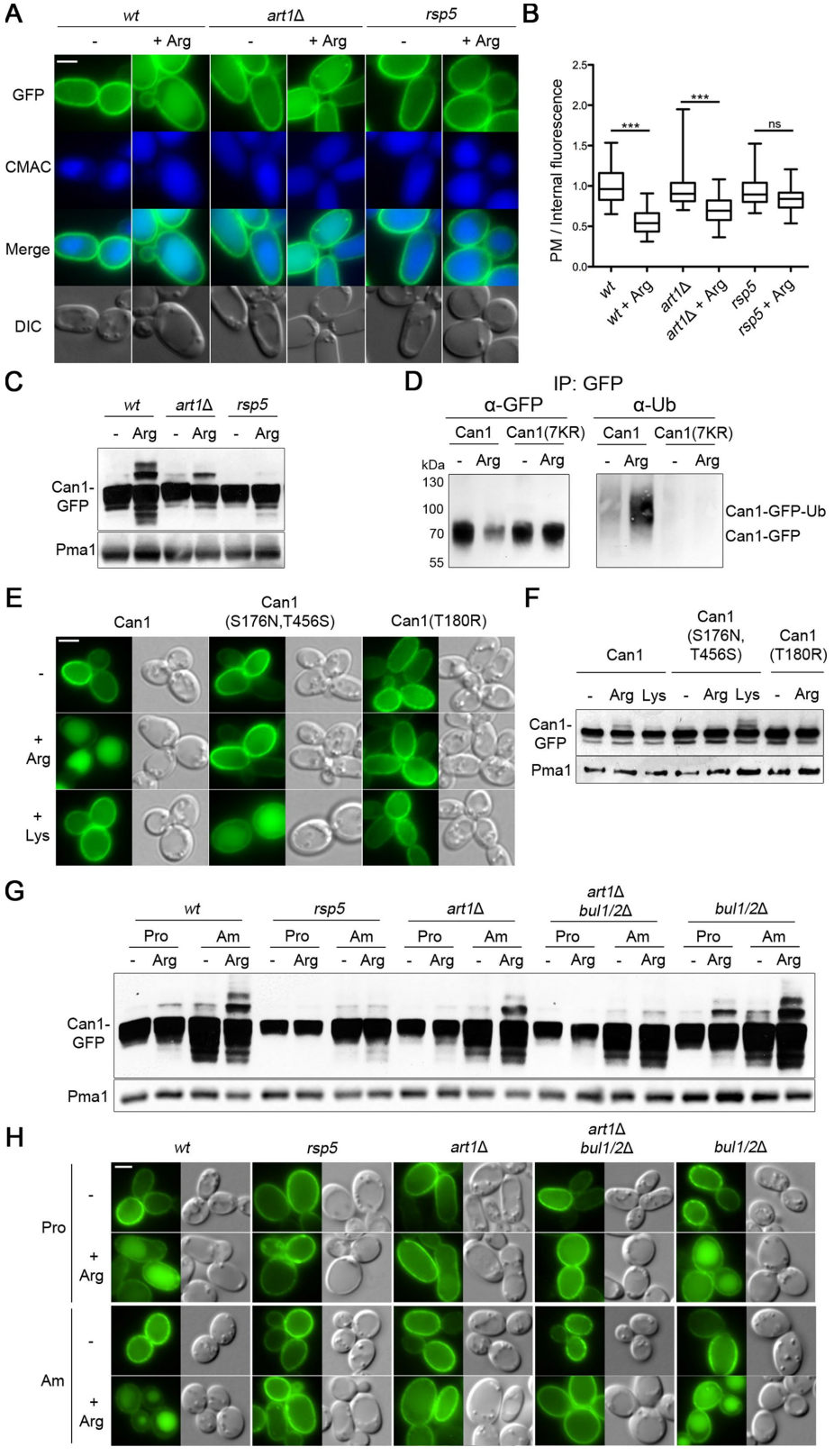

FIGURE 1: The Art1 and Bul α-arrestins promote Can1 ubiquitylation in response to arginine. (A) Strains (with *gap1*Δ *can1*Δ mutations) expressing Can1-GFP were grown on Gal Pro medium. *GAL*-promoter–driven expression of *CAN1-GFP* was repressed by addition of 3% Glu for 1.5 h. Arg (5 mM) was then added for 3 h. After CMAC staining, the cells were observed by epifluorescence microscopy. Scale bar here and below is 2 μm. (B) Plasma membrane (PM) to intracellular GFP fluorescence intensity ratios, for the experiment of A, are plotted ($n = 90$ cells). The horizontal midline represents the median, the box is bounded by the upper and lower quartiles, and the whiskers denote the maximal and minimal ratios. ***, $P < 0.001$; ns, nonsignificant, $P > 0.05$. Lower middle. (C) The strains of A were grown on Gal Pro; Glu was added for 0.5 h and then Arg for 30 min. Total protein extracts were probed with antibodies against GFP and Pma1. (D) Immunoprecipitation (IP), via GFP, of Can1-GFP or Can1(7KR)-GFP. Cells were grown in Gal Pro media, and glucose was added for 90 min, followed by 5 mM Arg for 25 min. After immunoprecipitation using GFP, extracts were probed with antibodies against GFP or Ub. (E, F) The effects of Arg or Lys addition to Gal Pro grown *gap1*Δ *can1*Δ *lyp1*Δ cells expressing Can1-GFP, Can1(S176N,T456S)-GFP, or Can1(T180R)-GFP were examined by epifluorescence microscopy (E) or by immunoblotting total protein extracts (F); conditions as in A and C, respectively. (G) Strains (with a *gap1*Δ mutation) expressing Can1-GFP were grown on Gal Pro or Gal Am medium. Glu was added for 30 min and then Arg for 15 min. Protein extracts were probed as in C. (H) Epifluorescence microscopy analysis of strains in G. Glu was added for 90 min and then Arg for 3 h. Quantification of the fluorescence signals is presented in Supplemental Figure S1.

Art1 α-arrestin thus appears sufficient to promote efficient Can1 down-regulation in response to Arg transport. Why Can1 is more efficiently targeted to the vacuole when ubiquitylated via Art1 than by Bul1/2 remains undetermined. Art1 and Bul1/2 might mediate different types of Can ubiquitylation. For example, short K63-linked Ub chains are known to be important for efficient targeting of internalized permeases to the vacuole (Lauwers *et al.*, 2010). Alternatively, during progression of the permease along the endocytic pathway to the vacuole, Art1 might maintain Can1 in a ubiquitylated state more efficiently than Bul1/2. Whatever the case may be, our results clearly show that the *bul1*Δ *bul2*Δ strain is perfectly suited for further investigating Art1-mediated ubiquitylation and down-regulation of Can1 upon substrate transport.

Art1 and Bul1/2 act via distinct N-terminal regions of Can1 to promote its ubiquitylation

The above results show that Art1-dependent ubiquitylation and down-regulation of Can1 are stimulated by substrate transport. We have previously proposed that structural changes in Can1 during transport catalysis might unveil a cytosolic region recognized by Art1, which would then recruit Rsp5 onto the permease and thereby cause

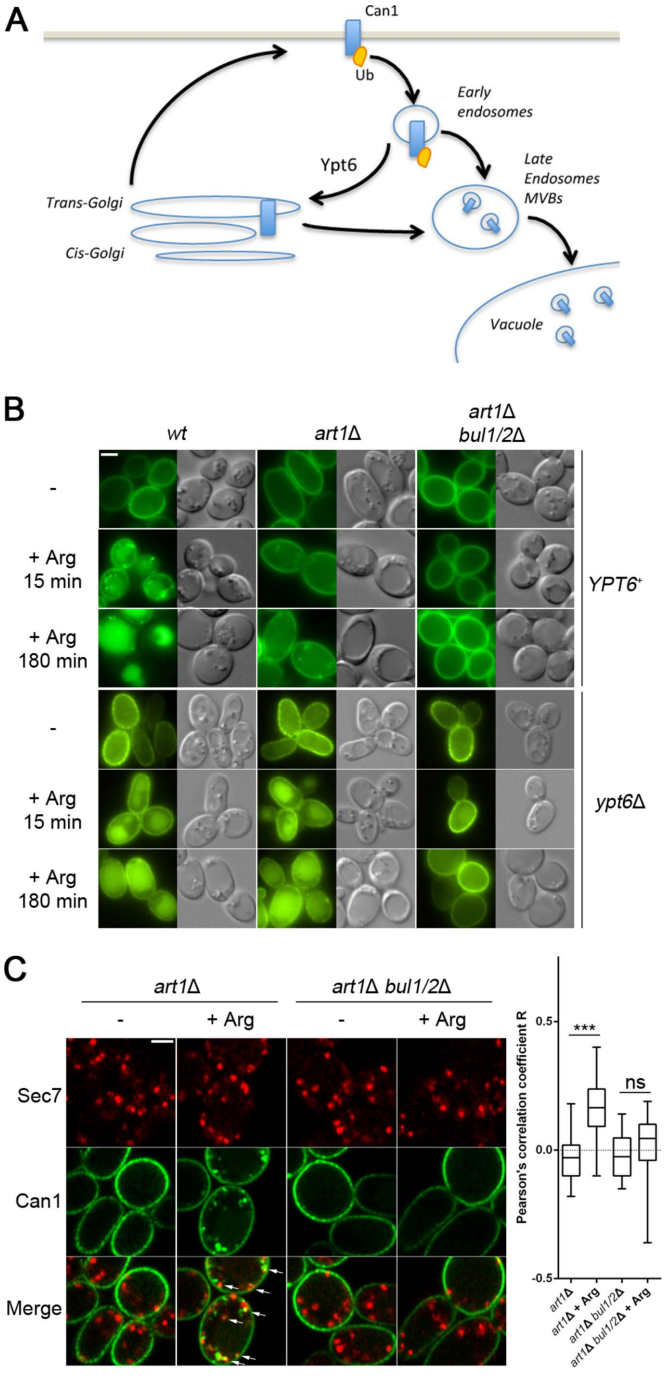

FIGURE 2: Can1 is internalized and recycles to the plasma membrane via the Golgi upon Arg addition to the *art1* mutant. (A) Scheme illustrating the role of Ypt6 Rab family small GTPase in recycling of membrane proteins from endosomes to the late Golgi complex. (B) Strains (all with *gap1*Δ *can1*Δ mutations) carrying or not a deletion of the *YTP6* gene, and expressing Can1-GFP, were grown in Gal Pro medium. Glu was added for 1.5 h and then Arg for the time indicated, before imaging by epifluorescence microscopy. (C) Strains expressing Can1-GFP and Sec7-mCherry were grown in Gal Pro medium. Glu was added for 1.5 h and then Arg for 15 min, before imaging by confocal microscopy. Arrows indicate sites of colocalization between Can1 and Sec7. Right: The Pearson's correlation coefficient for Can1-GFP and Sec7-mCherry are plotted ($n = 40$ cells). Representations as in Figure 1B.

its ubiquitylation (Ghaddar *et al.*, 2014b). To identify this region, we conducted an alanine-scanning mutagenesis of the Can1 cytosolic N-tail (Figure 3A). We focused on this tail because a Lyp1 permease variant carrying the N-tail of Can1 is reported to have acquired specific endocytic properties of Can1 (Lin *et al.*, 2008). In each N-tail mutant, three to four consecutive residues were replaced with alanines. The 23 isolated Can1 mutants were targeted to the plasma membrane, where most catalyzed Arg transport (Supplemental Figure S3, A–C). Four of the active Can1 mutants failed to be targeted to the vacuole after Arg addition (Supplemental Figure S3, A–C). The same result was obtained when these mutants were expressed in the *bul1*Δ *bul2*Δ mutant (Figure 3B and Supplemental Figure S3D), where Can1 ubiquitylation is mediated by Art1 alone. As one of these mutants was altered in the 42-KDEK-45 sequence, we hypothesized that Lys-42 and Lys-45 might be Ub acceptor lysines of Can1. Accordingly, we isolated a Can1(K42R,K45R) mutant and found it to be strongly protected against Arg-induced endocytosis via Art1 (a phenotype not due to loss of transport activity), whereas the Can1(K42R) and Can1(K45R) single mutants were targeted to the vacuole (Figure 3, C–E). Furthermore, the Can1(K42R,K45R) mutant showed strongly reduced Arg-induced ubiquitylation (Figure 3D). Ubiquitylation was not totally abolished, however. This suggests that Art1 can promote Can1 ubiquitylation on additional lysines, and that this residual ubiquitylation, like that mediated by Bul1/2, is not sufficient to target the permease efficiently to the vacuole. In support of this view, Can1 remained active but was fully protected against Arg-induced ubiquitylation and endocytosis when all seven lysines of the N-tail were replaced with arginines (Figure 3, F–H).

Three other mutants, altered in a sequence close to the first transmembrane domain (residues 70–81), also resisted Arg-induced down-regulation in the *bul1*Δ *bul2*Δ strain (Figure 3, A and B, and Supplemental Figure S3D). This region thus exhibits the properties expected of an Art1-binding site. Accordingly, this 70–81 region is similar in sequence to the Art1-binding site rich in acidic residues that has recently been found in Mup1, a methionine permease ubiquitylated via Art1 (Guiney *et al.*, 2016). Yet alanine substitutions in this region again reduced but did not abolish Art1-dependent ubiquitylation in response to Arg (Figure 4A). The residual detectable ubiquitylation, clearly insufficient to cause Can1 down-regulation (Figure 3B and Supplemental Figure, S3D), could reflect the existence of several contact points between Art1 and this 12-aa (amino acid) region; hence substitution of four consecutive residues might reduce without abolishing Art1 binding. Alternatively, Can1 could expose another Art1-binding site, sufficient for limited ubiquitylation but not for down-regulation (see also *Discussion*).

Next, to determine whether the Bul α-arrestins act via the same cytosolic region of Can1, we analyzed Arg-induced ubiquitylation of the active Can1 mutants in an *art1*Δ strain (Figure S3, E and F). Remarkably only two mutants, altered in a region (residues 62–69) just before the Art1-dependent site, failed to be ubiquitylated via Bul1/2 (Figure 4B). We then combined a substitution in this region (residues 66–69) with one altering the N-tail region required for Art1-mediated down-regulation (residues 74-77). This double mutant, when expressed in the wild-type strain producing Art1 and Bul1/2, remained active but proved to be very resistant to Arg-induced ubiquitylation and down-regulation (Figure 4, C–E). In conclusion, Art1 and Bul1/2 act via different though close regions of the N-tail of Can1 to promote Arg-induced Can1 ubiquitylation.

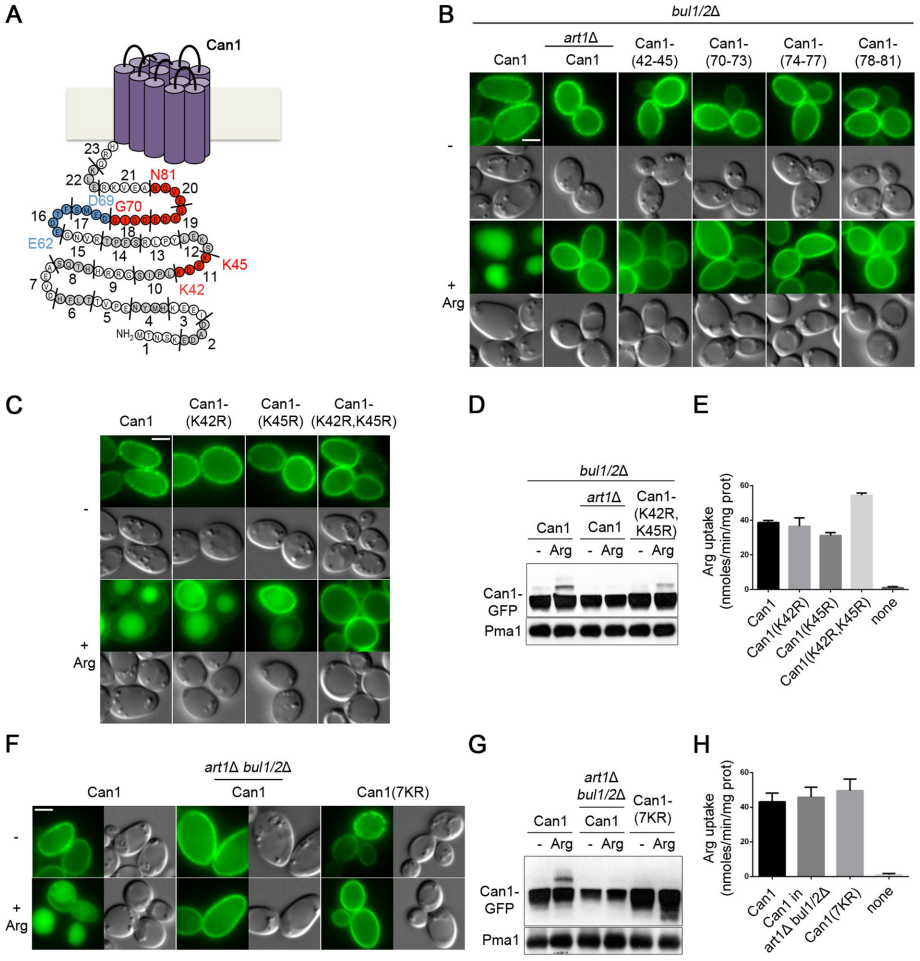

FIGURE 3: Lys-42 and Lys-45 are the main Ub-acceptors and required for efficient vacuolar sorting of Can1. (A) Schematic representation of the 23 mutants obtained by Ala-scanning mutagenesis of the N-tail of Can1. Mutants resistant to Art1-dependent endocytosis are shown in red, and those resistant to Bul1/2-dependent ubiquitylation in blue. The two main Ub-acceptor Lys residues required for efficient vacuolar sorting are also highlighted. See also Supplemental Figure S3 and Figure 4. (B) Strains (with *gap1*Δ *can1*Δ mutations) expressing Can1-GFP or Can1-GFP mutants carrying Ala-substitutions of the indicated residues of the N-tail were grown on Gal Am. Glu was added for 90 min and then Arg for 3 h before imaging as in Figure 1A. Quantifications are shown in Supplemental Figure S3D. (C, D, E) Epifluorescence microscopy analysis (C, as in Figure 1A) and immunoblots of total protein extracts (D, as in Figure 1G) of Gal Am grown strains (with *gap1*Δ *can1*Δ mutations) expressing Can1-GFP or the indicated Lys-to-Arg substitution alleles. For the immunoblot, cells were first grown in Raf Am and Gal was added for 1 h, Glu for 1.5 h and then Arg for 15 min. (E) C^{14}-Arg uptake measurements in a *gap1*Δ *can1*Δ *bul1/2*Δ strain expressing Can1-GFP, the corresponding mutants, or no Can1 protein. (F, G, H) Strains (with *gap1*Δ *can1*Δ mutations) expressing Can1-GFP or Can1-(7KR)-GFP were grown in Gal Am; experiments and conditions as in C, D, and E, respectively.

in this case both Gap1 and Can1 were down-regulated. (Figure 5, B and C). These results, together with the finding that inactive Can1 mutants resist Arg-induced endocytosis, show that Art1-mediated Can1 ubiquitylation and efficient down-regulation are stimulated only when the permease catalyzes substrate transport.

In a previous study we found the E184Q substitution in the substrate-binding site of Can1 to cause complete loss of transport activity (Ghaddar *et al.*, 2014a). Yet unlike other inactive Can1 forms, this variant was efficiently down-regulated by Arg. In contrast, the Can1(E184A) mutant, also inactive, displayed impaired down-regulation. It was thus hypothesized that Can1(E184Q) binds external Arg without being able to catalyze its uptake and that this binding is sufficient to trigger the conformational changes promoting Can1 recognition by Art1 (Ghaddar *et al.*, 2014b). To further assess this model, we tested the influence of the above-described mutations on Arg-elicited Can1(E184Q) down-regulation. Can1(E184Q) ubiquitylation and endocytosis proved to be largely defective in the *art1*Δ mutant but readily observed in the *bul1*Δ *bul2*Δ strain (Figure 5, E and F). A Can1 variant combining the E184Q, K42R, and K45R substitutions failed to be down-regulated by Arg, as did a variant combining E184Q with substitution of alanines for 74-EDED-77, which alters the putative Art1-targeted sequence in the N-tail region (Figure 5, E and F). These results are consistent with the hypothesis that Can1(E184Q), upon Arg binding, is recognized by Art1 and ubiquitylated. Next, in Can1(E184Q), we substituted arginine for Thr-180, located in the Can1 arginine-binding site. The T180R substitution is predicted with high confidence to prevent Arg binding via steric hindrance (Ghaddar *et al.*, 2014a). Surprisingly, it did not abolish Arg-elicited ubiquitylation and down-regulation of Can1(E184Q) (Figure 5, G and H). Another unexpected observation was that the inactive Can1(E184Q) was not down-regulated by Arg when expressed in the *gap1*Δ *can1*Δ strain defective for Arg uptake, but was efficiently down-regulated in the *gap1*Δ and *can1*Δ single-mutant strains, able to assimilate external Arg (Figure 5I). Furthermore, this endocytosis of Can1(E184Q) was not caused by some interaction with Can1 or Gap1 undergoing Arg-induced down-regulation because it also occurred in the *gap1*Δ *can1*Δ strain expressing the Can1(7KR)-mCherry that remained stable at the cell surface after Arg addition (Figure 5J). These results rather show that uptake of external Arg is essential to Arg-induced down-regulation of Can1(E184Q).

To account for these observations, we considered the following model. Two conditions would have to be fulfilled for efficient Can1 down-regulation in response to Arg transport. First, the putative Art1-binding site present in the N-tail of Can1, likely hidden when

Specific inactive Can1 mutants permanently expose the N-terminal region targeted by Art1

Art1 and Bul1/2 are regulated by TORC1 via the Npr1 kinase (Figure 5A). When Am is added to Pro-grown cells, TORC1 is stimulated, causing inhibition of Npr1 through rapamycin-sensitive phosphorylation (Figure 5B). As a result, Art1 and Bul1/2 are activated by inhibition relief (Schmidt *et al.*, 1998; MacGurn *et al.*, 2011; Merhi and André, 2012). This, however, proved insufficient to trigger Art1-mediated ubiquitylation of Can1 and its efficient targeting to the vacuole (Figure 5, C and D). In contrast, Gap1 was efficiently down-regulated after Am addition (Figure 5C). Arg addition to Pro-grown cells also caused TORC1-dependent phosphorylation of Npr1, and

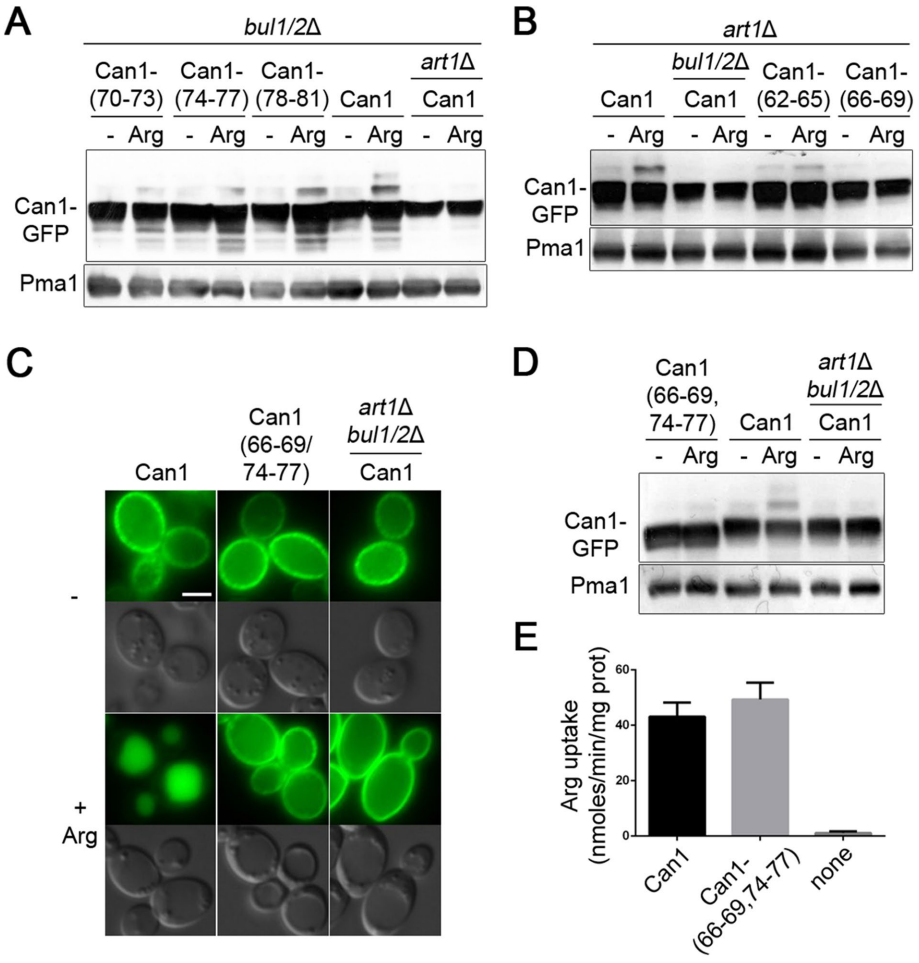

FIGURE 4: Art1 and Bul1/2 act via distinct N-terminal regions of Can1 to promote its ubiquitylation. (A) Strains (all with *gap1*Δ *can1*Δ mutations) expressing Can1-GFP or Can1-GFP mutants carrying Ala-substitutions of the indicated residues of the N-tail 70–81 region were grown on Gal Am. Glu was added for 0.5 h and then Arg for 15 min. Protein extracts were probed as in Figure1C. (B) Strains (with *gap1*Δ *can1*Δ mutations) expressing Can1-GFP or Can1-GFP mutants carrying Ala-substitutions of the indicated residues of the N-tail 62–69 region were examined as in A. See also Supplemental Figure S3F. (C, D, E) Epifluorescence microscopy analysis (C), immunoblotting (D), and C^{14}-Arg uptake measurements (E) of Can1-GFP and a mutant carrying Ala substitutions of 66–69 and 74–77 residues, conditions as in Figure 3, F, G, and H, respectively.

the permease is catalytically inert, would have to be exposed to the cytosol. This occurs when Can1 undergoes the conformational changes coupled to transport catalysis. Second, Art1 would have to be stimulated via TORC1-mediated inhibition of the Npr1 kinase (MacGurn *et al.*, 2011). This occurs, for example, after Arg uptake into Pro-grown cells. The particularity of the inactive variant Can1(E184Q) would be that it is more populated in the particular conformation exposing the Art1-binding site and normally adopted by the wild type only during catalysis of Arg transport. Stimulation of TORC1 after Arg uptake would therefore be sufficient to promote Can1(E184Q) down-regulation (Figure 6A). To test this model, we added Am to Pro-grown cells expressing Can1(E184Q). Remarkably, Am addition did trigger Art1-dependent ubiquitylation of the mutant permease and its targeting to the vacuole, a phenotype not observed with either wild-type Can1 or the Can1(E184A) mutant (Figure 6, B and C, and Supplemental S4A). Another prediction of the model is that Can1(E184Q), but neither Can1 nor Can1(E184A), should be constitutively targeted to the vacuole in an Art1-dependent manner in the *npr1*Δ mutant grown on Pro medium. This was also confirmed (Figure 6D and Supplemental Figure S4B). Furthermore, mutations altering the main Ub acceptor residues Lys-42 and Lys-45 or the Art1-targeted 70–81 region protected Can1(E184Q) against down-regulation induced by Am addition or a lack of Npr1 kinase (Figure 6, B–D, and Supplemental Figure S4, A and B). In further support of the view that Can1(E184Q) favors a different fold, we found it to be more sensitive than wild-type Can1 to trypsinolysis under non-denaturing conditions (Supplemental Figure S4C). In conclusion, these results suggest that substrate transport, or the E184Q substitution in the substrate-binding site, impacts the N-tail structure of Can1 in such a manner that the region between residues 70 and 81 is unveiled, allowing Art1, once activated by TORC1, to promote Can1 ubiquitylation and down-regulation (Figure 6A).

We next reasoned that transport-elicited unveiling of the 70–81 cytosolic region could in principle be caused also by substitutions in the N-tail itself. Mutants harboring such substitutions should behave like Can1(E184Q), that is, they should be stable at the cell surface in Pro-grown cells and down-regulated after Am addition. As the 23 N-tail mutants had been tested previously in Pro-grown cells, before and after Arg addition (Supplemental Figure S3A), we further tested their ability to undergo Art1-dependent, Am-induced endocytosis (Supplemental Figure S4D). One mutant, altered in the 87-ELK-89 sequence, remarkably displayed this phenotype (Figure 6E). This sequence lies between the first transmembrane segment (TM) and the putative binding site of Art1 (Figure 3A, mutant 22). Its replacement with alanines caused a drastic loss of transport activity (Supplemental Figure S3C), suggesting that it is important for transport catalysis. A model compatible with these observations is that the integrity of the 87-ELK-89 sequence is required to mask the nearby Art–binding site and that structural rearrangements accompanying transport catalysis cause the region recognized by Art1 to become exposed to the cytosol.

Transition of Can1 to the inward-facing conformation unveils its Art1-targeted sequence

We next sought to gain more mechanistic insight into how the structural rearrangements elicited by substrate transport or by the E184Q substitution are transmitted to the N-tail of Can1 to unmask the putative binding site of Art1. Can1 belongs to the amino-acid-polyamine-organocation (APC) superfamily, the second largest superfamily of secondary transporters, which includes the well-known LeuT amino-acid transporter (Gournas *et al.*, 2016). These proteins adopt a common fold, the LeuT fold, consisting of two inverted repeats of five helical TMs comprising the substrate-binding site. Like that mediated by transporters of other families, APC-mediated

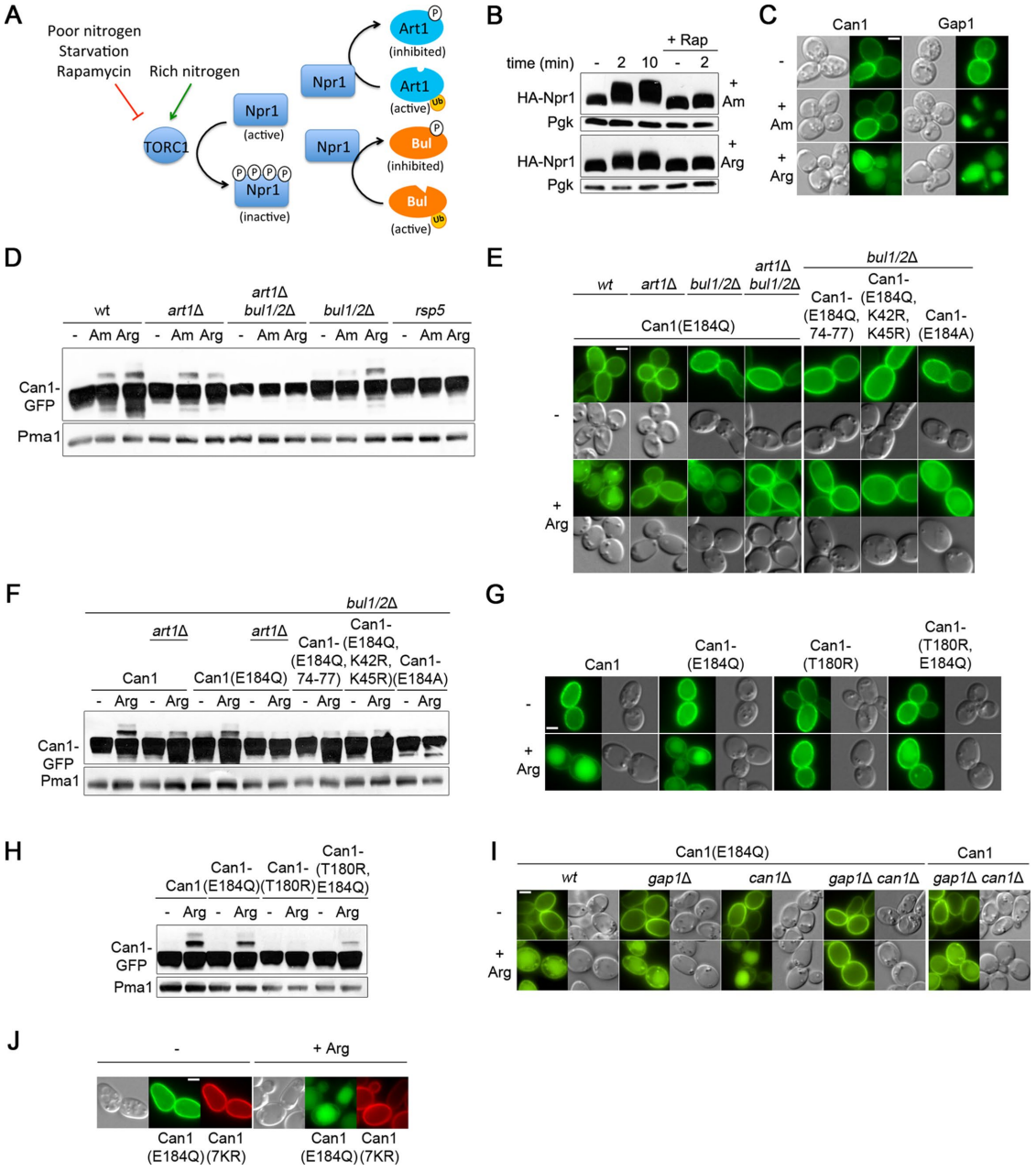

FIGURE 5: The inactive Can1(E184Q) mutant is down-regulated upon Arg uptake. (A) Schematic representation of the regulation of the Art1 and Bul α-arrestins by nitrogen availability via the TORC1 pathway. (B) Immunoblots of total protein extracts of a wild-type strain expressing HA-Npr1. Samples with or without rapamycin addition 30 min before Am or Arg addition were collected and probed with anti-HA antibodies. (C) Epifluorescence microscopy analysis of Gal Pro grown *gap1*Δ *can1*Δ cells expressing Can1-GFP or Gap1-GFP. Glu was added for 1.5 h and then Arg or Am for 3 h. (D) Strains (with *gap1*Δ *can1*Δ mutations) expressing Can1-GFP were grown on Gal Pro. Glu was added for 30 min and then Arg or Am for 15 min. Total protein extracts were probed as in Figure 1C. (E) Epifluorescence microscopy analysis (as in Figure 1A) and (F) immunoblotting (as in Figure 1C) of Can1-GFP and the indicated mutants in Gal Pro grown strains (with a *gap1*Δ mutation). (G) Epifluorescence microscopy analysis (as in Figure 1A) and (H) immunoblotting of Can1-GFP and the indicated mutants; conditions as in E and F, respectively. (I) Epifluorescence microscopy analysis (as Figure 1A) of the corresponding strains expressing Can1-GFP or Can1(E184Q)-GFP; conditions as in E. (J) Epifluorescence microscopy analysis (as in Figure 1A) of a *gap1*Δ *can1*Δ strain expressing Can1(7KR)-mCherry and Can1(E184Q)-GFP.

transport occurs via alternating access to the substrate-binding site, through the adoption of outward-facing (OF) and inward-facing (IF) conformations, the OF-to-IF transition being promoted by occlusion of the substrate-binding site (Krishnamurthy and Gouaux, 2012).

We have recently shown that the high-resolution structure of the bacterial arginine/agmatine AdiC transporter provides a good template for building structural models of Can1 and for analyzing its arginine-binding site, which includes Glu-184 (Ghaddar *et al.*, 2014a).

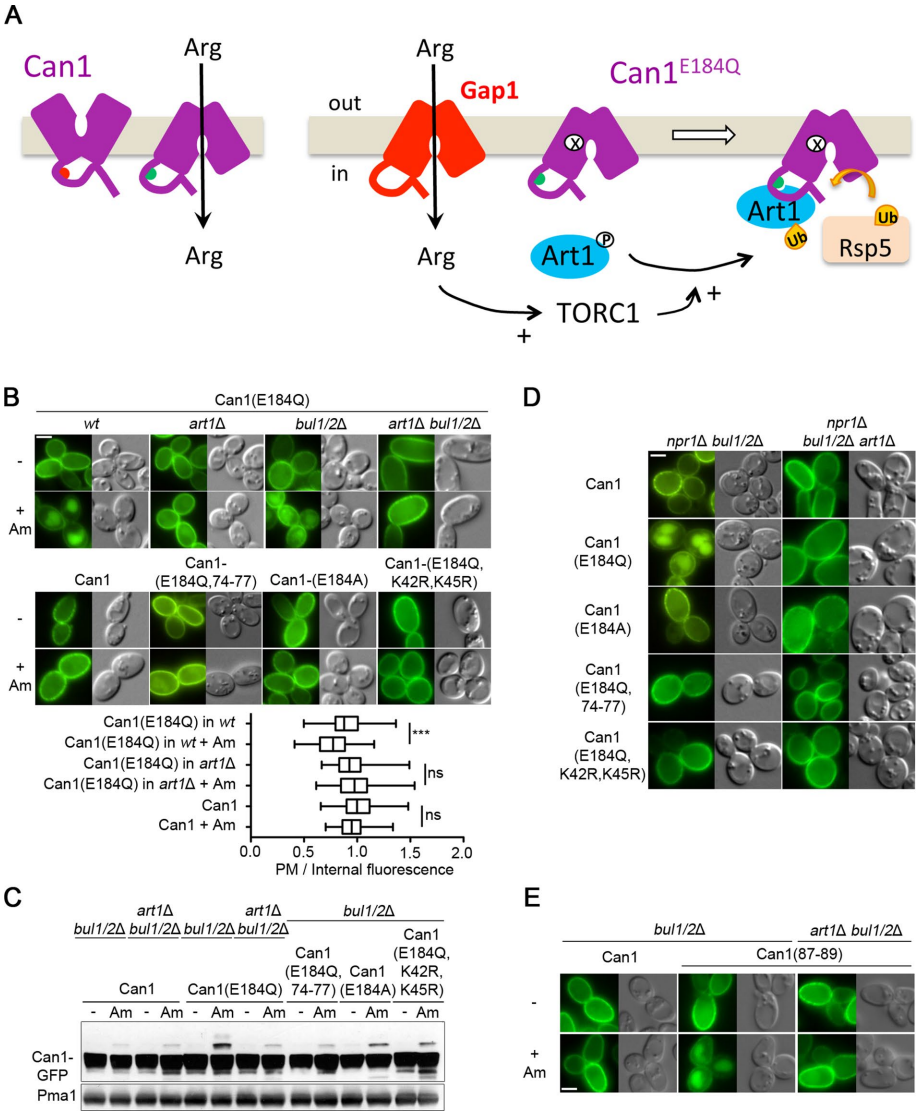

FIGURE 6: TORC1-mediated activation of Art1 is sufficient to down-regulate the inactive Can1(E184Q) and Can1(87-ELK-89>AAA) mutants. (A) Hypothetical model for the mechanism of Art1-mediated down-regulation of Can1(E184Q) following Gap1-mediated Arg uptake. (B) Strains (with *gap1*Δ *can1*Δ mutations) expressing Can1(E184Q) and the *gap1*Δ *can1*Δ *bul1/2*Δ strain expressing GFP-fused wild-type or mutant Can1 (as indicated) were grown on Gal Pro. Glu was added for 1.5 h and then Am for 3 h, before imaging. The PM-to-intracellular-GFP fluorescence intensity ratios (as in Figure 1B) are plotted for the main conditions ($n = 60$ cells). Quantifications for other control strains are shown in Supplemental Figure S4A. (C) The same strains were grown on Gal Pro, Glu was added for 0.5 h and then Am for 20 min. Protein extracts were probed as in Figure 1C. (D) Strains expressing Can1-GFP or the indicated mutants were grown in Gal Pro. Glu was added for 1.5 h before imaging as in Figure 1A. See also Supplemental Figure S4B. (E) Strains expressing Can1-GFP or the mutant carrying Ala substitutions of residues 87–89 were examined as in Figure 5C. See also Supplemental Figure S4D.

We therefore generated and compared multiple three-dimentional (3D) models of Can1 and Can1(E184Q), in the OF open, OF occluded, and IF conformations (see *Materials and Methods*). As the region required for Art1-dependent Can1 down-regulation is located in the N-tail connected directly to TM1, we examined the positioning of this TM, which includes a kink in its middle. Superimposition of the Can1 models showed no significant differences in the positioning of TM1 between the OF open and OF occluded models, whereas a significant repositioning of the TM1 portion oriented toward the cytosol was observed in the IF conformation (Figure 7A). This resulted in a rotation of ~60 deg of the TM1 part near the N-tail, thereby entailing a large movement of the 87-ELK-89 sequence, which is required for masking the Art1-binding site (Figure 7A). The above observations suggest that the transient Can1 conformation affecting the structure of its N-tail likely corresponds to the IF state. Consistently, no significant movements of the nearby TM1 have been observed in the crystal structures of several APC proteins during transition from the OF open to the OF occluded state, whereas TM1 undergoes a large movement during the shift to the IF state (Gao *et al.*, 2010; Krishnamurthy and Gouaux, 2012; Krammer *et al.*, 2016). Thus a substrate-induced switch of Can1 to the IF conformation, through repositioning of the TM1 portion facing the cytosol and of the nearby ELK sequence required to mask the 70–81 region, could trigger exposure of this region to the cytosol, allowing its recognition by Art1.

We next sought to determine whether the E184Q substitution in TM3 could favor a more populated IF conformation. We thus focused on the potential interactions of Gln-184 or Glu-184, the latter in its charged or protonated form, with surrounding residues of other TMs. Particular attention was paid to H-bonds, as the Gln side chain has the capacity to form up to four H-bonds via its amide group. For each of the three conformational states of Can1, the H-bonds established by residue 184 were examined in 10 structural models. Interestingly, we found the E184Q substitution to cause a global increase of H-bonds in the IF models (Figure 7B). Most of these H-bonds were formed with Ile-386 and Asn-393 of TM8, but bonds were also formed with Thr-104 of TM1. TM3 was thus bridged with TM8 and/or TM1. In the OF open and OF occluded conformations, the E184Q substitution did not significantly alter the pattern of H-bonding with other TMs (Figure 7B). The extra H-bonds established by Gln-184 in the IF state might thus contribute to increasing the stability of Can1(E184Q) in this conformation.

To further evaluate the hypothesis that an IF conformation is more populated in Can1(E184Q), we analyzed the influence of additional substitutions. We have previously reported that the S176N substitution impedes the Arg transport activity of Can1 (Ghaddar *et al.*, 2014a). Molecular docking analysis indicated that this lack of activity is caused not only by a loss of H-bonds between Ser-176 and the Arg substrate, but also, in the OF occluded state, by steric hindrance due to the bulkier Asn side chain with several surrounding residues. Lys, which is smaller, was predicted to be able to bind to the substrate-binding pocket of Can1(S176N). Yet it failed to be transported, likely because of the steric hindrance effect. In particular, in seven out of 10 models the presence of the bulkier Asn-176 side chain affected the positioning of Trp-177,

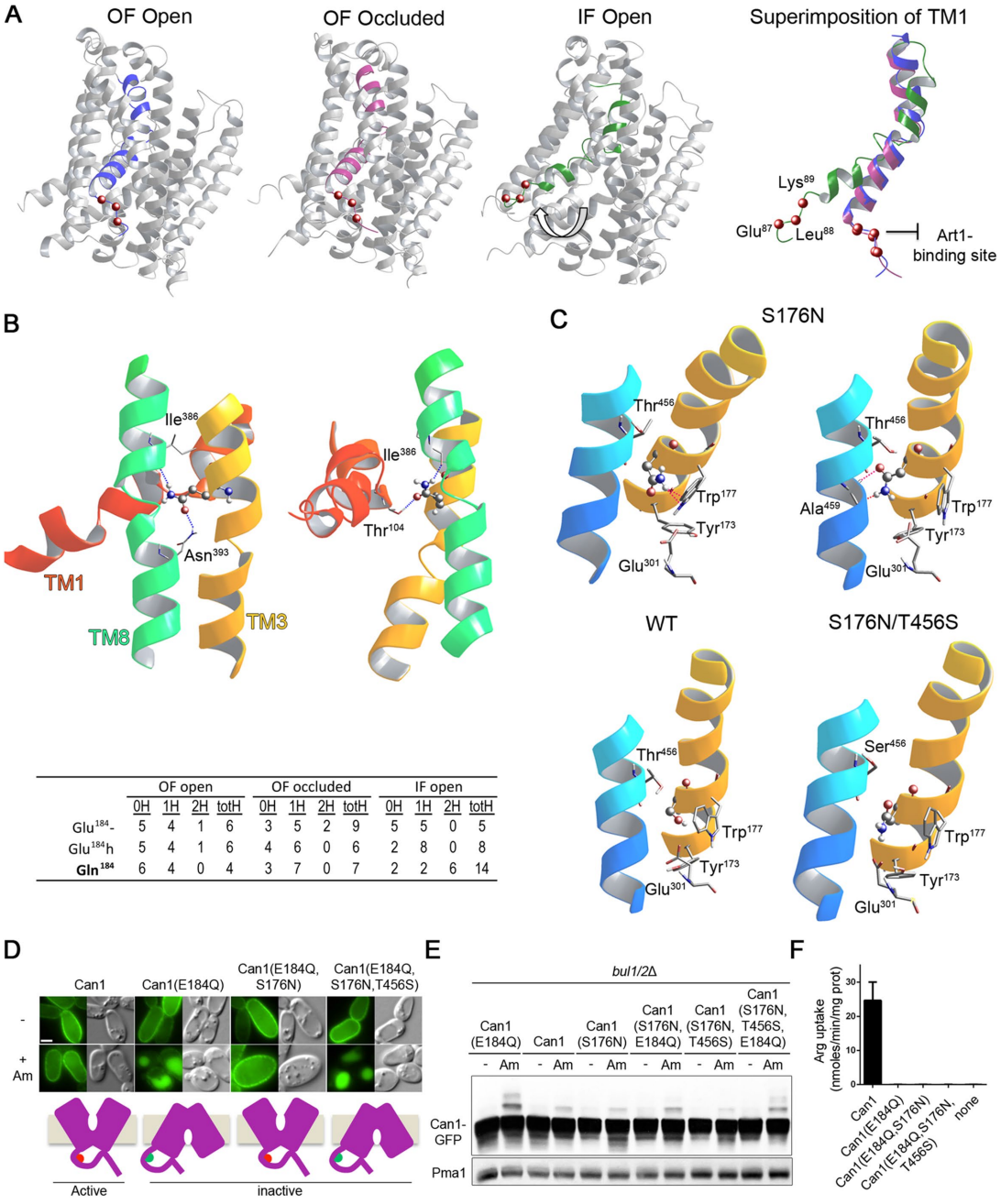

	OF open				OF occluded				IF open			
	0H	1H	2H	totH	0H	1H	2H	totH	0H	1H	2H	totH
Glu^{184}-	5	4	1	6	3	5	2	9	5	5	0	5
Glu^{184}h	5	4	1	6	4	6	0	6	2	8	0	8
Gln^{184}	6	4	0	4	3	7	0	7	2	2	6	14

FIGURE 7: The E184Q substitution is predicted to stabilize Can1 in an IF conformation. (A) Left, 3D models of Can1 in the OF open, OF occluded, and IF open states, highlighting a shift (white arrow) of TM1 in the IF open conformation. Right, Close-up of TM1 colored in blue, purple, and green, respectively, in the OF open, OF occluded, and IF open conformations. The location of the 87–89 sequence is shown as red balls marking the Cα position of the residues. (B) Top, view of the surroundings of Gln-184 in two 3D models of substrate-free IF open Can1(E184Q). Gln-184 is shown as balls and sticks and the residue hydrogen-bonding to it is shown as sticks. A ribbon diagram depicting neighboring residues of TM1, TM3, and TM10 is also shown. Hydrogen bonds formed by Gln-184 are shown as blue broken lines. Bottom, summary table of the analysis of H-bonds formed by residue at position 184 in structural models of Can1(E184Q) and wild-type Can1, with Glu-184 in the protonated (Glu-184h) or charged (Glu-184-) form, in the OF open, OF occluded and IF open conformations. 0H, 1H, 2H: number of Can1 models (out of 10) with no, one, or two H-bonds established by the side chain of residue 184 (in TM3) with residues of other TMs. totH: total number of H-bonds established by the side chain of residue 184 with other TMs in the 10 analyzed Can1 models. (C) Close-up view of the region encompassing residue 176 in representative OF occluded models of Can1, Can1(S176N,T456S), and Can1(S176N). In two Can1(S176N) models, pink broken lines show steric hindrance between the N176 side chain, depicted as balls and sticks, and neighboring residues, including those of the middle (W177) and distal (Y173, E301, W464) gates. Portions of TM1, TM3, and TM10 are depicted as ribbons. (D) Epifluorescence microscopy analysis of a *gap1*Δ *can1*Δ *bul1/2*Δ strain expressing Can1-GFP or the indicated mutant grown on Gal Pro. Glu was added for 1.5 h and then Am for 3 h. (E) immunoblots of cell extracts from the strains of D grown on Gal Pro. Glu was added for 0.5 h and then Am for 0.5 h. (F) ^{14}C-Arg uptake measurements in a *gap1*Δ *can1*Δ strain expressing the indicated Can1 mutant. See also Supplemental Figure S5.

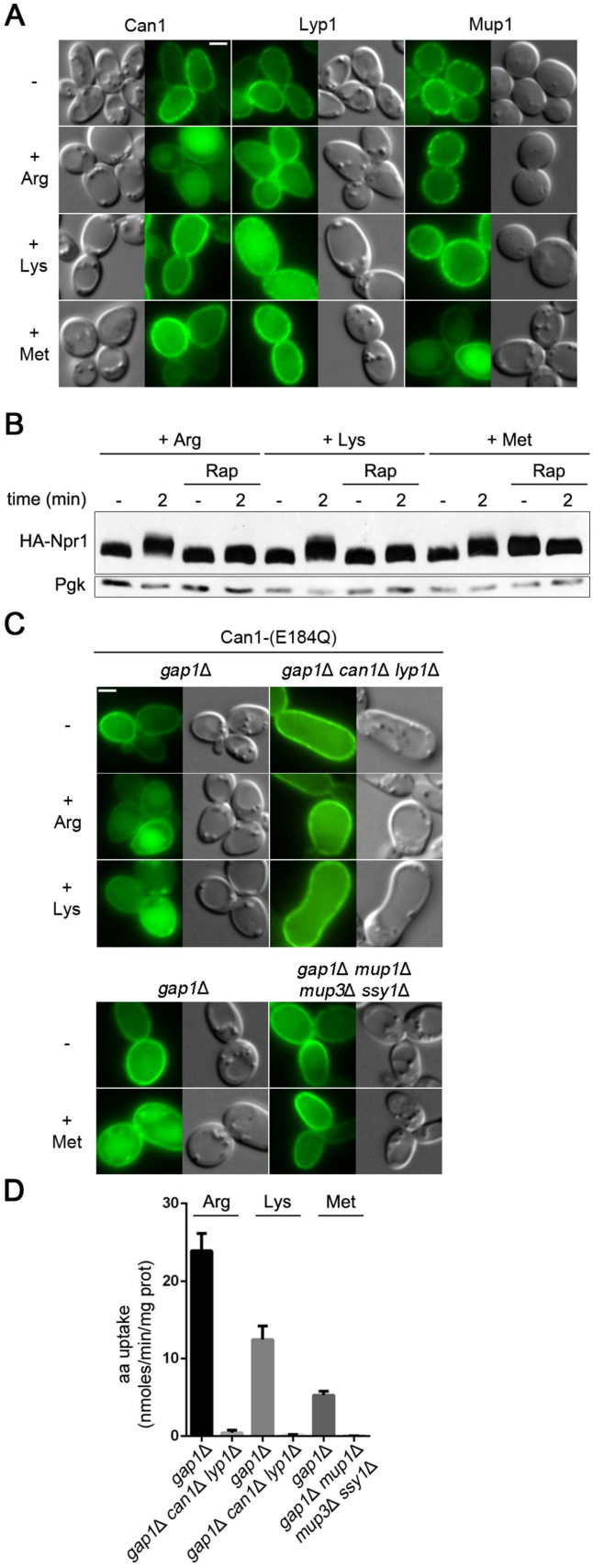

FIGURE 8: Substrate-transport–elicited unveiling of permease cytosolic regions brings specificity to Art1-mediated ubiquitylation. (A) Epifluorescence microscopy analysis of a strain expressing Mup1-GFP and of a *gap1Δ* strain expressing Can1-GFP or Lyp1-GFP. For Can1-GFP, Gal Pro was used and Glu was added for 1.5 h. For Lyp1-GFP and Mup1-GFP, Glu Pro was used. Arg, Lys, or Met was added for 3 h before observation. (B) Immunoblotting of total protein extracts as in Figure 5B. Arg, Lys, or Met was added in rapamycin-treated and untreated wild-type cells. (C) Epifluorescence microscopy analysis and (D) ^{14}C-amino acid uptake measurements on the indicated strains expressing Can1(E184Q) and grown in Gal Pro. For microscopy, Glu was added for 1.5 h and then Arg, Lys, or Met for 3 h.

Tyr-173, or Glu-301 (Figure 7C), these being highly conserved residues of the middle and distal gates (Gournas *et al.*, 2016). Interestingly, interactions of the substrate with the corresponding residues of AdiC and subsequent opening of the distal gate are proposed to be crucial for the transition to an IF conformation (Gao *et al.*, 2010). Hence, because of steric hindrance the S176N substitution is predicted to inhibit the transition to a more IF conformation (Ghaddar *et al.*, 2014a). We thus introduced the S176N substitution into Can1(E184Q). Remarkably, we found the resulting Can1(E184Q,S176N) variant to have lost the ability to undergo Art1-dependent ubiquitylation and vacuolar sorting in response to Am (Figure 7, D and E). This genetic epistasis effect was specific to S176N, as it was not observed when the T180R substitution, affecting only substrate binding (Ghaddar *et al.*, 2014a), was introduced into Can1(E184Q) (Figure 5G and Supplemental Figure S5A). We finally introduced into Can1(E184Q,S176N) yet another substitution, T456S. Thr-456 is located in TM10, in very close proximity to Ser-176. As mentioned above, Can1(S176N,T456S) can catalyze Lys transport, likely because the steric effect of Asn-176 is relieved (Figure 7C), a void being formed between the smaller Ser and the nearby Asn-176 (Supplemental Figure S5B; Ghaddar *et al.*, 2014a). Interestingly, the ability to undergo Am-induced ubiquitylation and endocytosis is restored in the Can1(E184Q,S176N,T456S) triple mutant (Figure 7, D and E).

In conclusion, the data support the model that Can1(E184Q) is stabilized in an IF state constantly exposing the N-terminal 70–81 region targeted by Art1, that an additional S176N substitution epistatically blocks the permease in the OF state, where this N-tail sequence is no longer exposed, and that this effect can be relieved by T456S. It is noteworthy that all three above-described Can1 variants are unable to transport Arg (Figure 7F) and would thus appear to differ only in their ability to expose or not the cytosolic region targeted by Art1.

Substrate-transport-elicited unveiling of transporter cytosolic regions brings specificity to ubiquitylation via the same TORC1-activated α-arrestin

Art1 is involved in the Ub-dependent endocytosis of at least two other specific permeases: the methionine (Met) permease Mup1 and the Lys permease Lyp1 (Lin *et al.*, 2008; Keener and Babst, 2013). Like Can1, Mup1 and Lyp1 underwent efficientdown-regulation when their own substrate was provided to Pro-grown cells, but they remained stable at the cell surface if the substrate of another permease was present (Figure 8A). Furthermore, like Arg addition, the addition of Met or Lys to Pro-grown cells was found to activate TORC1, since it caused rapamycin-sensitive phosphorylation of the Npr1 kinase (Figure 8B). One can thus assume Art1 to be stimulated after addition of Met or Lys. Why Can1 does not undergo down-regulation upon addition of one of these amino acids is likely due to masking of its N-terminal Art1-binding site. In support of this view, we found Can1(E184Q) to be efficiently down-regulated in response to Met or Lys (Figure 8C). Furthermore, this down-regulation was impaired in mutant strains unable to incorporate the amino acid triggering TORC1 stimulation (Figure 8, C and D). These results indicate

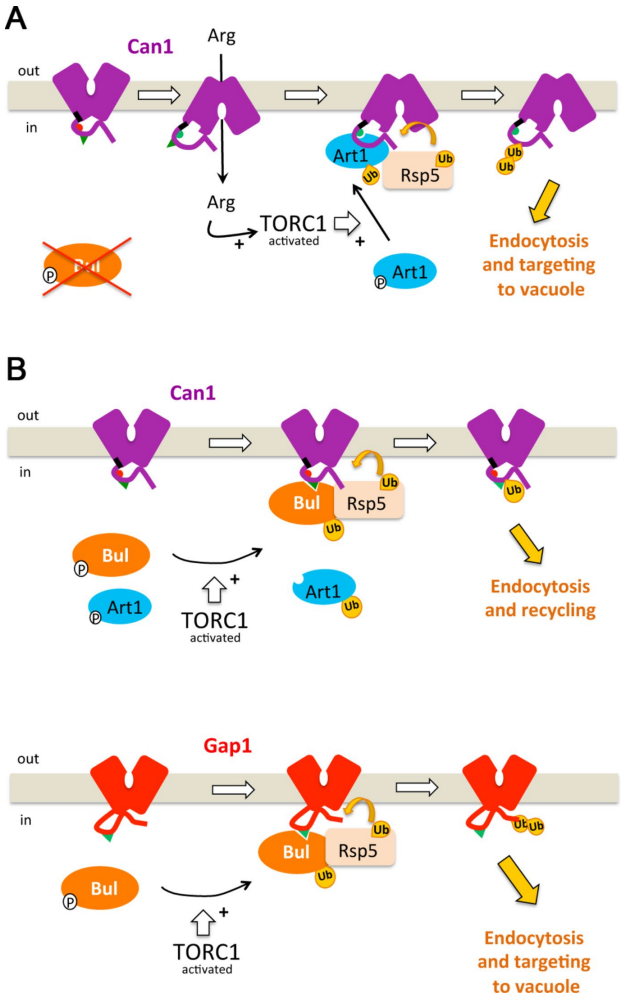

FIGURE 9: Model of the mechanisms governing ubiquitylation and endocytosis of yeast amino acid permeases. (A) Art1- and Rsp5-mediated ubiquitylation and down-regulation of Can1 permease in response to substrate transport and TORC1 activation, as in the mutant lacking the Bul α-arrestins, for example. In the absence of substrate, the short ELK sequence (black) close to TM1 is oriented toward the core of the transporter and interacts with cytoplasmic loops, structuring the remaining tail so that the binding site for Art1 (aa 70–81, red hemicycle) is masked. In the presence of Arg, a transient switch of Can1 to an IF conformation, via repositioning of TM1 and the ELK tripeptide, causes a structural rearrangement unmasking the binding site for Art1 (now green). Arg uptake also stimulates TORC1, which activates Art1. Once activated, Art1 can recognize the unveiled binding site. This results in Rsp5-mediated Can1 ubiquitylation, mainly on Lys-42 or Lys-45. (B) Ubiquitylation and endocytosis of Gap1 and Can1 in response to TORC1 stimulation. Activation of TORC1 stimulates the Art1 and Bul α-arrestins. Once activated, the Buls can act through a permanently exposed region of the Gap1 N-tail (residues 20–35), causing its ubiquitylation on Lys-9 or Lys-16. This modification efficiently targets Gap1 to the vacuole. The activated Buls also recognize a permanently exposed binding site in the Can1 N-tail (residues 62–69), causing its ubiquitylation. This modification does not efficiently target the internalized Can1 to the vacuole. The TORC1-activated Art1 does not efficiently recognize Can1 because its binding site remains masked.

that substrate-transport-elicited exposure of an α-arrestin–binding site brings specificity to the mechanism by which the same TORC1-regulated α-arrestin causes endocytosis of multiple permeases.

DISCUSSION

Substrate-transport–elicited endocytosis is a very common control mechanism of transporters, though poorly understood at the molecular level. In this study we have molecularly dissected the mechanism triggering Ub-dependent endocytosis and targeting to the vacuole of Can1, the yeast arginine permease, in response to transport catalysis. We have found that two conditions must be fulfilled for Can1 to undergo this down-regulation (Figure 9A). First, the α-arrestin Art1 promoting Rsp5-dependent ubiquitylation of Can1 must be stimulated via the TORC1/Npr1 signaling cascade. This occurs, for example, upon Arg uptake into the cell. Second, Can1 must unveil a region of its N-tail (aa 70–81) targeted by activated Art1. Our structural modeling analysis and experimental data suggest that this occurs when Can1 transiently adopts an IF state during transport catalysis. Importantly, unveiling of this N-tail 70–81 sequence can become permanent by two types of mutations in Can1: 1) upon substitution of three consecutive residues (87-ELK-89) located at the intersection between TM1 and the N-tail and 2) when Can1 harbors in its substrate-binding site the E184Q substitution predicted by structural modeling to favor an IF conformation. The effect of E184Q is counteracted by the S176N substitution stabilizing Can1 in the OF state via steric hindrance, unless the latter is relieved by an additional T456S substitution. The structural rearrangement allowing Can1 in the IF state to expose its N-tail 70–81 region likely involves repositioning of the TM1 portion oriented toward the cytosol, together with the directly connected 87-ELK-89 tripeptide. A molecular scenario compatible with our data is that in the OF state, this tripeptide interacts with other cytosolic regions of Can1, for example, internal loops, and that this interaction is broken upon the shift to the IF state or when the tripeptide is replaced with alanines. In both situations, this results in a structural rearrangement of the N-tail and exposure of the 70–81 region. Remarkably, data provided by the structural modeling of other APC superfamily transporters similarly underscored a conformation-dependent interaction between specific basic residues preceding TM1 and other cytosolic regions of the transporters. More specifically, Lys-79 of the human serotonin transporter, hSERT, and Lys-60 of the dopamine transporter of *Drosophila melanogaster*, hDAT, were predicted to form a salt bridge with residues located at the end of TM8 (Kniazeff *et al.*, 2008; Fenollar-Ferrer *et al.*, 2014). This salt bridge forms only in the OF state and is believed to contribute to the stabilization of this conformation. Furthermore, the linkage seems to break upon transition to the IF state and, similar to our findings about Can1, this breaking would be favored by the movement of TM1 during the OF-to-IF transition. The essential roles of the 87-ELK-89 sequence of Can1 in transport activity and masking the 70–81 region might likewise reflect a role of Lys-89 in the formation of a salt bridge with another cytosolic region of the transporter stabilizing it in the OF conformation. It is thus tempting to propose that several APC family transporters, from yeast to mammals, share specific structural remodeling features during transition from the OF to IF states and that these rearrangements govern interactions with various cytosolic factors in response to substrate transport. One might also anticipate that for Can1 to be efficiently recognized by Art1, the IF state adopted during transport catalysis must be sufficiently populated. Can1 might thus switch back to the OF state with limited efficiency, in order to increase the probability of molecular contacts with Art1. Importantly, this view could explain the very particular phenotype of Can1(T456S). This variant displays an abnormally high *V*max of transport but largely resists transport-elicited endocytosis (Ghaddar *et al.*, 2014b), perhaps because the permease more rapidly switches back to the OF state after substrate release. This model is supported

by structural modeling data suggesting that the T456S substitution facilitates structural transitions of the transport cycle (Ghaddar *et al.*, 2014a). The model might also apply to UapA, a purine transporter of *Aspergillus nidulans* subject to transport-elicited endocytosis, as transporter mutants behaving like Can1(T456S) have been described (Gournas *et al.*, 2010; Alguel *et al.*, 2016). Regarding residue Glu-184, whose replacement with glutamine is proposed to stabilize Can1 in an IF state, one should mention that Arg transport via Can1 is coupled to H^+ symport (Opekarová *et al.*, 1993) and that pKa calculations suggest that Glu-184 may exist in a charged and a protonated state (Ghaddar *et al.*, 2014a). The E184Q substitution might thus mimic a natural Glu-184 protonation coupled to Arg translocation that could be part of the mechanism favoring transition to the IF state. As Can1(E184Q) is inactive, one might also consider that subsequent deprotonation of Glu-184 is necessary to allow Can1 to release Arg into the cytosol and/or to switch back to an OF open state.

Other amino acid permeases such as Mup1 and Lyp1 also undergo efficient substrate-transport–elicited, Art1- and Rsp5-dependent endocytosis (Lin *et al.*, 2008; Keener and Babst, 2013). Down-regulation of Mup1 and Lyp1, like that of Can1, likely involves structural remodeling on the cytosolic side of the transporter. A recent study has indeed identified in Mup1 an N-terminal sequence close to TM1, rich in acidic residues, that is essential to Art1-dependent ubiquitylation and down-regulation of the permease in response to excess substrate. This sequence is most likely the binding site of Art1, as substitutions within it can be compensated by specific *art1* mutations (Guiney *et al.*, 2016). This study further noted that the N-tail of Can1 also contains a region rich in acidic residues and thus potentially recognized by Art1. Our results show that the depicted region in fact includes the adjacent sequences needed for Art1- and Bul-dependent endocytosis, respectively. As in the case of Can1, the N-tail sequence found in Mup1 might become accessible to Art1 upon shifting of the permease to the IF state. Our data further indicate that substrate-transport–elicited endocytosis of Mup1 and Lyp1 likely requires, like that of Can1, additional activation of Art1 via TORC1. We propose that this double-lock mechanism adds specificity to a down-regulation process affecting distinct permeases targeted by the same α-arrestin. For example, arginine uptake activates Art1 via TORC1 without causing Mup1 or Lyp1 endocytosis. Furthermore, down-regulation of these permeases likely occurs only when the amount of amino acid entering the cell is sufficient to activate TORC1. This seems to be a very efficient means of fine-tuning the abundance and activity of permeases and coordinating them with cell metabolism to achieve perfect homeostasis (Savir *et al.*, 2017) and avoid the potential toxicity of substrates accumulating in excess in the cell. For instance, we have found Arg to be toxic to cells in which Can1 resists down-regulation (Supplemental Figure S6). The reduced growth caused by Arg when Can1 fails to be down-regulated suggests that cells undergo a stress. In a previous study, we reported that Can1 is ubiquitylated under various stress conditions, in a manner only partially dependent on Art1 (Crapeau *et al.*, 2014). The residual ubiquitylation we observed for most Can1 mutants resistant to down-regulation might thus result from stimulation of this stress-induced pathway.

The conditions causing down-regulation of Can1, Lyp1, and Mup1 differ from those promoting Gap1 down-regulation (Figure 9B): TORC1-dependent stimulation of the Bul α-arrestins is sufficient to promote efficient Gap1 ubiquitylation and endocytosis (Merhi and André, 2012). This down-regulation depends on a short region in the Gap1 N-tail, likely to be a constantly exposed binding site for the activated Bul proteins. Interestingly, the Bul α-arrestins can promote Gap1 down-regulation even when not stimulated by TORC1. This happens, for instance, when substitutions are introduced into specific cytosolic regions of the permease, likely causing an additional Bul-binding site to be unmasked (Ghaddar *et al.*, 2014b). Ubiquitylation of amino acid permeases thus seems to obey combinatorial interaction rules according to which α-arrestins, stimulated *or not* via TORC1, target permease regions permanently facing the cytosol *or* unveiled during transport catalysis (Figure 9).

Our data also reveal an unexpected contribution of the activated Bul α-arrestins to Can1 ubiquitylation (Figure 9B). These proteins act through another N-tail region of the permease (aa 62–69), near the Art1-targeted 70–81 sequence. The Bul-targeted sequence seems constantly exposed to the cytosol, as the TORC1-activated Buls can use it even when Can1 does not catalyze uptake. Yet the resulting ubiquitylation, detected in the *art1Δ* mutant, promotes very limited Can1 down-regulation, as the internalized Can1 mainly recycles to the cell surface via the Golgi. Our results therefore show that Art1, also sufficient for Can1 ubiquitylation and initial internalization, is crucial for the targeting of the internalized permease to the vacuole, a view consistent with the previously reported localization of Art1 at the Golgi (Lin *et al.*, 2008). Previous work has also shown that the Rod1/Art4 α-arrestin controls the fate of internalized transporters by promoting their Golgi-to-vacuole sorting (Becuwe and Léon, 2014). This illustrates the complexity of the mechanisms governing the ubiquitylation of plasma membrane transporters, which may involve several α-arrestins recognizing unmasked or constantly exposed cytosolic regions and acting at several successive steps of the endocytic pathway.

It is very likely that transporters from more complex organisms including mammals are also regulated via substrate-transport–elicited stabilization of specific conformations promoting their interaction with cytosolic factors. For instance, the human serotonin transporter in the IF conformation tends to be phosphorylated, which increases its transport activity (Zhang *et al.*, 2016). The ARRDC proteins of animal cells are structural orthologues of the yeast α-arrestins (Alvarez, 2008). Recent studies have shown some ARRDCs to interact with NEDD4-type Ub ligases similar to yeast Rsp5 and to act at various steps of the endocytic pathway to promote Ub-dependent down-regulation of several receptors (Patwari and Lee, 2012). Furthermore, the Glut1 transporter is negatively controlled by the ARRDC protein TXNIP (Wu *et al.*, 2013). As transport-elicited endocytosis likely controls transporters in all eukaryotic species in order to avoid excess accumulation of substrates, it will be important to determine whether the involved mechanisms are similar to those described here for the yeast Can1 permease and to evaluate their importance in the proper functioning of transporters in their physiological context.

MATERIALS AND METHODS

Yeast strains and growth conditions

All yeast strains used in this study (Supplemental Table S1) derive from strain Σ1278b, apart from the strain expressing Mup1-GFP that derives from BY4741. The *npi1-1* strain is a viable *rsp5* mutant in which a Ty element inserted in the upstream control region of the gene results in severely reduced expression of *RSP5* (Hein *et al.*, 1995). Cells were grown at 29°C on a minimal buffered medium, pH 6.1 (Jacobs *et al.*, 1980), with galactose (Gal; 3%), raffinose (Raf; 3%), or glucose (Glu; 3%) as carbon source. The nitrogen sources present in the growth media were ammonium, in the form of $(NH_4)_2SO_4$, (10 mM), proline (10 mM), or arginine (5 mM). The final concentrations of substances added to solid or liquid media were arginine (5 mM), lysine (5 mM), methionine (1 mM), $(NH_4)_2SO_4$ (50 mM), rapamycin (200 ng/ml), canavanine (10 μg/ml). The *CAN1-GFP* and *GAP1-GFP* genes were expressed under the control of the *GAL* promoter. Cells were grown on galactose medium, and glucose

was added for 0.5 or 1.5 h before cell transfer to conditions inducing transporter ubiquitylation/endocytosis. The *LYP1* and *MUP1* genes were expressed under their respective natural promoters.

Plasmids used in this study

The plasmids used in this study are listed in Supplemental Table S2. Novel plasmids were constructed by in vivo recombination in yeast. For the alanine-scanning mutagenesis, we applied a previously described method (Merhi *et al.*, 2011) where the overlapping sequences of PCR fragments were 40 base pairs long and contained the sequence for introducing three or four consecutive alanine substitutions. Each plasmid was purified by cloning into *Escherichia coli* and verified by sequencing. Nucleotide sequences are available upon request.

Epifluorescence and confocal microscopy

The subcellular location of GFP-tagged transporters was determined with an Eclipse 80i (Nikon) epifluorescence microscope equipped with a 100× differential interference contrast, numerical aperture (NA) 1.40 Plan-Apochromat objective (Nikon) and appropriate fluorescence light filter sets. Images were captured with a DS-Qi1Mc-U3 (Nikon) digital camera and NIS-Elements 4.3 acquisition software (Nikon). For confocal microscopy, images were acquired with a ZEIS LSM710 equiped with Airyscan and an 100x differential interference contrast, NA 1.45 Plan-Apochromat objective, using ZEN 2.1 SP2 software. Images were processed with ImageJ software (National Institutes of Health, Bethesda, MD) and annotated with Photoshop CS5 (Adobe Systems). Cells derived from exponentially growing early logarithmic phase liquid cultures were laid on a thin layer of 1% agarose and observed at room temperature. In each figure, typically only a few cells representative of the whole cell population, observed in at least two independent biological replicate experiments, are shown. In some key experiments, fluorescence quantification was performed. Labeling of cell vacuoles was done in liquid medium with 250 µM CellTracker Blue CMAC dye (Life Technologies, Carlsbad, CA) for 15 min. Cells were pelleted and resuspended before imaging.

Fluorescence quantification

The fluorescence intensity of Can1-GFP was quantified using ImageJ software. Two ellipses, one outlining the cell and another on the inside, excluding the plasma membrane (PM), were drawn manually ($n > 60$ cells). The ratio of PM-to-internal-mean-pixel intensity for each cell population is presented in box-and-whisker plots. The obtained values in fact underestimate the actual PM-to-internal ratios in the analyzed cell populations, because the internal fluorescence includes both vacuolar and other intracellular organelles and also the background fluorescence of the cells due to epifluorescence microscopy. We measured internal instead of vacuolar fluorescence intensities because the vacuole increases in size after Arg addition and because internalized Can1 can localize to nonvacuolar intracellular compartments. For colocalization experiments, the Pearson's correlation coefficient value (R) was determined for at least 40 single cells from each condition, using a custom-made script for the coloc2 plug-in of ImageJ. Prism software, one-way analysis of variance (ANOVA) with the nonparametric Kruskal-Wallis test, and Dunn's multiple-comparison post hoc analyses were used to assess the significance of PM-to-internal-fluorescence ratio and Pearson's correlation coefficient value differences.

Protein extracts and Western blotting

For immunoblot analyses, crude cell extracts were prepared and analyzed by SDS–PAGE as previously described (Hein *et al.*, 1995). Proteins were transferred to a nitrocellulose membrane (Protran; Perkin Elmer) and probed with a mouse monoclonal anti-GFP (Roche), anti-hemagglutinin (anti-HA) (Roche), anti-yeast 3-phosphoglycerate kinase (anti-PGK; Invitrogen), anti-Ub (Santa Cruz; sc8017), or rabbit monoclonal anti-Pma1 (Ghaddar *et al.* 2014a), Primary antibodies were detected by enhanced chemiluminescence (Roche) after treatment with horseradish-peroxidase-conjugated anti-mouse or anti-rabbit immunoglobulin (Ig) G secondary antibody (Sigma). Signals were detected with CL-Xposure film (Thermo Scientific). Films were scanned and annotated with Photoshop CS5.

Immunoprecipitation of Can1-GFP

This experiment is based in the one described in Merhi and Andre (2012) and Guiney *et al.* (2016), with modifications. Briefly, 12,5 OD cells were collected by filtration and frozen at –80°C. Cells were resuspended in 800 µl RIPA buffer (50 mM Tris HCl, pH 7.5, 150 mM NaCl, 20 mM NaF, 1 mM EDTA, 0.5 mM EGTA [ethylene glycol-bis[β-aminoethyl ether]-*N*,*N*,*N*′,*N*′-tetraacetic acid]), supplemented with fresh 1 mM dithiothreitol, 1 mM phenyl-methyl-sulfonyl fluoride, Fungal protease inhibitor coctail (Sigma-Aldrich, St. Louis, MO), and 20 mM *n*-ethylmaleimide, and broken by glass beads by vortexing for 10 min at 4°C. Membranes were solubilized by the addition of 100 µl of 10% NP-40 and 4% sodium deoxycholate in RIPA buffer, followed by a 30 min incubation at 4°C. Cell debris was pelleted by a 5 min centrifugation at 3000 rpm. The supernatant was incubated with preequilibrated anti-GFP microbeads (µMACS GFP isolation kit; Milteniy biotec) for 1 h at 4°C. The beads were washed four times with 200 µl RIPA buffer, and Can1-GFP was eluted from the beads in elution buffer, according to the manufacturer's intructions.

Limited trypsin digestion analysis

This experiment was carried out as described previously (Lauwers *et al.*, 2007). Briefly, cells were lysed with glass beads in 200 µl buffer (50 mM HEPES, pH 7.5, 300 mM NaCl). A total membrane fraction was generated by centrifugation at 100,000 × *g* for 60 min in a SW55 Ti rotor (Beckman Coulter, Fullerton, CA). Membrane proteins were resuspended in the same buffer and a final concentration of 0.5 µg/µl was incubated with trypsin at 100 or 200 µg/ml concentration. Samples were incubated for different times with trypsin and the reaction was stopped by adding trypsin inhibitor type I-S from soybean (Sigma-Aldrich). A control reaction was run for 30 or 60 min in the absence of trypsin. Proteins were precipitated by adding 10% trichloroacetic acid (TCA), resuspended in sample buffer, and Can1-GFP was analyzed by Western blotting with an anti-GFP antibody.

Permease activity assays

Permease transport activities were determined by measuring the initial uptake rate (20–90 s) of ^{14}C-labeled amino acids (Perkin-Elmer, Boston, MA) diluted with unlabeled amino acids to a final concentration of 10–30 µM, as previously described (Ghaddar *et al.*, 2014a). Error bars indicate SEs determined for at least two independent biological replicates.

Structural modeling of Can1 variants

Three-dimensional structural models of Can1 and Can1(E184Q) were built in the OF open, OF occluded, and IF conformational states (10 models for each variant in each state) by comparative modeling with Modeller9v1 (Fiser and Sali, 2003). Crystallographic 3D structures of AdiC (PDB [Protein Data Bank] IDs: 3OB6 and 3L1L) (Gao *et al.*, 2010; Kowalczyk *et al.*, 2011) were used as templates to construct the OF open and occluded models, respectively. As no experimental 3D structure of AdiC in the IF state has been determined so far, we used as a template the IF conformations of AdiC

extracted from a molecular dynamics simulation of the AdiC transport cycle (Krammer *et al.*, 2016). Each model was then submitted to the Protein Preparation Wizard protocol of Schrodinger Suite 2015 (Schrödinger Release 2015-1). Missing hydrogens were added, and this was followed by optimization of H-bonds and energy minimization of the models. The protonation state of each titratable residue was chosen according to a PROPKA prediction at pH = 7.0. In Can1 models comprising Glu-184, this residue was considered in both its neutral and charged forms. This led to 20 models per state, hence 60 in total. Finally, using Prime software from Schrodinger, each of the 60/30 (E184/Q184) 3D models was used to predict the E184/Q184 side chain and to energetically minimize it. The Schrodinger maestro graphics interface was used to analyze all models.

ACKNOWLEDGMENTS

We thank Laure Twyffels and Stelios Gkionis for implementing the fluorescence quantification scripts for ImageJ, Catherine Jauniaux for her excellent technical assistance, R. Wedlich-Söldner for providing the Mup1-GFP strain, and members of the laboratory for fruitful discussions. M.P. is a senior research associate and C.G. and E.-M.K. are postdoctoral researchers of the the Fonds de la Recherche Scientifique de Belgique (F.R.S-FNRS). E.S. and C.B. are fellows of the Fonds pour la formation a la Recherche dans l'Industrie et dans l'Agriculture (FRIA). This work was supported by a Fonds de la Recherche Scientifique Médicale (FRSM) grant (3.4.592.08.F).

REFERENCES

Alguel Y, Amillis S, Leung J, Lambrinidis G, Capaldi S, Scull NJ, Craven G, Iwata S, Armstrong A, Mikros E, *et al.* (2016). Structure of eukaryotic purine/H(+) symporter UapA suggests a role for homodimerization in transport activity. Nat Commun 7, 11336.

Alvarez CE (2008). On the origins of arrestin and rhodopsin. BMC Evol Biol 8, 222.

Alvaro CG, O'Donnell AF, Prosser DC, Augustine AA, Goldman A, Brodsky JL, Cyert MS, Wendland B, Thorner J (2014). Specific α-arrestins negatively regulate Saccharomyces cerevisiae pheromone response by down-modulating the G-protein coupled receptor Ste2. Mol Cell Biol 34, 2660–2681.

Becuwe M, Léon S (2014). Integrated control of transporter endocytosis and recycling by the arrestin-related protein Rod1 and the ubiquitin ligase Rsp5. Elife 3, e03307.

Becuwe M, Vieira N, Lara D, Gomes-Rezende J, Soares-Cunha C, Casal M, Haguenauer-Tsapis R, Vincent O, Paiva S, Léon S (2012). A molecular switch on an arrestin-like protein relays glucose signaling to transporter endocytosis. J Cell Biol 196, 247–259.

Crapeau M, Merhi A, André B (2014). Stress conditions promote yeast Gap1 permease ubiquitylation and down-regulation via the arrestin-like Bul and Aly proteins. J Biol Chem 289, 22103–22116.

Fenollar-Ferrer C, Stockner T, Schwarz TC, Pal A, Gotovina J, Hofmaier T, Jayaraman K, Adhikary S, Kudlacek O, Mehdipour AR, *et al.* (2014). Structure and regulatory interactions of the cytoplasmic terminal domains of serotonin transporter. Biochemistry 53, 5444–5460.

Fiser A, Sali A (2003). Modeller: generation and refinement of homology-based protein structure models. Methods Enzymol 374, 461–491.

Gao X, Zhou L, Jiao X, Lu F, Yan C, Zeng X, Wang J, Shi Y (2010). Mechanism of substrate recognition and transport by an amino acid antiporter. Nature 463, 828–832.

Ghaddar K, Krammer E-M, Mihajlovic N, Brohée S, André B, Prévost M (2014a). Converting the yeast arginine Can1 permease to a lysine permease. J Biol Chem 289, 7232–7246.

Ghaddar K, Merhi A, Saliba E, Krammer E-M, Prévost M, André B (2014b). Substrate-induced ubiquitylation and endocytosis of yeast amino acid permeases. Mol Cell Biol 34, 4447–4463.

Gournas C, Amillis S, Vlanti A, Diallinas G (2010). Transport-dependent endocytosis and turnover of a uric acid-xanthine permease. Mol Microbiol 75, 246–260.

Gournas C, Prévost M, Krammer E-M, André B (2016). Function and regulation of fungal amino acid transporters: insights from predicted structure. Adv Exp Med Biol 892, 69–106.

Guiney EL, Klecker T, Emr SD (2016). Identification of the endocytic sorting signal recognized by the Art1-Rsp5 ubiquitin ligase complex. Mol Biol Cell 27, 4043–4054.

Hein C, Springael JY, Volland C, Haguenauer-Tsapis R, André B (1995). *NPI1*, an essential yeast gene involved in induced degradation of Gap1 and Fur4 permeases, encodes the Rsp5 ubiquitin-protein ligase. Mol Microbiol 18, 77–87.

Jacobs P, Jauniaux JC, Grenson M (1980). A cis-dominant regulatory mutation linked to the argB-argC gene cluster in Saccharomyces cerevisiae. J Mol Biol 139, 691–704.

Keener JM, Babst M (2013). Quality control and substrate-dependent downregulation of the nutrient transporter Fur4. Traffic 14, 412–427.

Kniazeff J, Shi L, Loland CJ, Javitch JA, Weinstein H, Gether U (2008). An intracellular interaction network regulates conformational transitions in the dopamine transporter. J Biol Chem 283, 17691–17701.

Kowalczyk L, Ratera M, Paladino A, Bartoccioni P, Errasti-Murugarren E, Valencia E, Portella G, Bial S, Zorzano A, Fita I, *et al.* (2011). Molecular basis of substrate-induced permeation by an amino acid antiporter. Proc Natl Acad Sci USA 108, 3935–3940.

Krammer E-M, Ghaddar K, André B, Prévost M (2016). Unveiling the mechanism of arginine transport through AdiC with molecular dynamics simulations: the guiding role of aromatic residues. PLoS ONE 11, e0160219.

Krishnamurthy H, Gouaux E (2012). X-ray structures of LeuT in substrate-free outward-open and apo inward-open states. Nature 481, 469–474.

Lauwers E, Erpapazoglou Z, Haguenauer-Tsapis R, André B (2010). The ubiquitin code of yeast permease trafficking. Trends Cell Biol 20, 196–204.

Lauwers E, Grossmann G, André B (2007). Evidence for coupled biogenesis of yeast Gap1 permease and sphingolipids: essential role in transport activity and normal control by ubiquitination. Mol Biol Cell 18, 3068–3080.

Lauwers E, Jacob C, André B (2009). K63-linked ubiquitin chains as a specific signal for protein sorting into the multivesicular body pathway. J Cell Biol 185, 493–502.

Léon S, Haguenauer-Tsapis R (2009). Ubiquitin ligase adaptors: regulators of ubiquitylation and endocytosis of plasma membrane proteins. Exp Cell Res 315, 1574–1583.

Lin CH, MacGurn JA, Chu T, Stefan CJ, Emr SD (2008). Arrestin-related ubiquitin-ligase adaptors regulate endocytosis and protein turnover at the cell surface. Cell 135, 714–725.

Luo Z, Gallwitz D (2003). Biochemical and genetic evidence for the involvement of yeast Ypt6-GTPase in protein retrieval to different Golgi compartments. J Biol Chem 278, 791–799.

MacGurn JA, Hsu P-C, Emr SD (2012). Ubiquitin and membrane protein turnover: from cradle to grave. Annu Rev Biochem 81, 231–259.

MacGurn JA, Hsu P-C, Smolka MB, Emr SD (2011). TORC1 regulates endocytosis via Npr1-mediated phosphoinhibition of a ubiquitin ligase adaptor. Cell 147, 1104–1117.

Merhi A, André B (2012). Internal amino acids promote Gap1 permease ubiquitylation via TORC1/Npr1/14-3-3-dependent control of the Bul arrestin-like adaptors. Mol Cell Biol 32, 4510–4522.

Merhi A, Gérard N, Lauwers E, Prévost M, André B (2011). Systematic mutational analysis of the intracellular regions of yeast Gap1 permease. PLoS ONE 6, e18457.

Nikko E, Marini AM, André B (2003). Permease recycling and ubiquitination status reveal a particular role for Bro1 in the multivesicular body pathway. J Biol Chem 278, 50732–50743.

Nikko E, Sullivan JA, Pelham HR B (2008). Arrestin-like proteins mediate ubiquitination and endocytosis of the yeast metal transporter Smf1. EMBO Rep 9, 1216–1221.

Opekarová M, Caspari T, Tanner W (1993). Unidirectional arginine transport in reconstituted plasma-membrane vesicles from yeast overexpressing CAN1. Eur J Biochem 211, 683–688.

Patwari P, Lee RT (2012). An expanded family of arrestins regulate metabolism. Trends Endocrinol Metab 23, 216–222.

Savir Y, Martynov A, Springer M (2017). Achieving global perfect homeostasis through transporter regulation. PLoS Comput Biol 13, e1005458.

Schmidt A, Beck T, Koller A, Kunz J, Hall MN (1998). The TOR nutrient signalling pathway phosphorylates NPR1 and inhibits turnover of the tryptophan permease. EMBO J 17, 6924–6931.

Springael JY, André B (1998). Nitrogen-regulated ubiquitination of the Gap1 permease of *Saccharomyces cerevisiae*. Mol Biol Cell 9, 1253–1263.

Wu N, Zheng B, Shaywitz A, Dagon Y, Tower C, Bellinger G, Shen CH, Wen J, Asara J, McGraw TE, *et al.* (2013). AMPK-dependent degradation of TXNIP upon energy stress leads to enhanced glucose uptake via GLUT1. Mol Cell 49, 1167–1175.

Zhang Y-W, Turk BE, Rudnick G (2016). Control of serotonin transporter phosphorylation by conformational state. Proc Natl Acad Sci USA 113, E2776–E2783.